Simulation-Based Evaluation of WAAS Performance: Risk and Integrity Factors

Samuel P. Pullen, Per K. Enge, and Bradford W. Parkinson

Department of Aeronautics and Astronautics
Stanford University

BIOGRAPHIES

Sam Pullen is a Ph.D. student and research assistant in the Gravity Probe-B project at Stanford University. An S.B. Graduate of MIT, he conducts research on spacecraft design for reliability and robust control design along with studies of GPS integrity performance.

Per Enge is a Research Professor of Aeronautics and Astronautics at Stanford University. A Ph.D. graduate of the University of Illinois, his research focuses on WAAS aircraft landing applications. He previously taught at WPI and is the ION Satellite Division Chairman.

Brad Parkinson is a Professor of Aeronautics and Astronautics at Stanford University and is the program manager for the Gravity Probe-B relativity gyro experiment. He served as the first Program Director of the GPS Joint Program Office and was instrumental in the system's development.

ABSTRACT

The Wide Area Augmentation System (WAAS) uses an array of monitor stations that combine to compute GPS user corrections over the Continental U.S. Preliminary experiments have concluded that ionospheric spatial decorrelation is the most significant of the WAAS error sources. Recent data on ionospheric errors has been combined into a probability model that describes the likelihood of rare-event ionospheric decorrelations over a range of conditions. Using this model and simpler models for troposphere and other errors, computer simulations of WAAS performance for randomly located users, using the MITRE ionospheric grid algorithm, have been conducted.

These simulation studies focused on performance sensitivity to various algorithm parameters and the potential of user-based RAIM algorithms to meet the WAAS availability and integrity requirements. It was found that both standard residual statistics and a new method of projecting spatial decorrelations from the gridpoint estimates show promise in improving overall WAAS performance. Remaining ionospheric uncertainty prevents us from meeting all the requirements, but more detailed experiments will allow us to improve our models and offer better performance.

1.0 Introduction

The Wide Area Augmentation System (or WAAS) has in the past few years grown from a theoretical study into an FAA proposal to build a network of about 20 monitor stations (or WRS's) coordinated by a master station (WMS) which computes DGPS corrections and transmits them to users from the ground or through geosynchronous satellites, which also serve as GPS ranging sources [1]. The components of this system could be in place by 1997. WAAS development is being supported by experiments at MITRE and Stanford University which use smaller test networks of 3 or 4 monitors to gather accuracy data [2,4,13]. These preliminary tests have provided data that allows us to better model wide-area DGPS performance for the full-scale system.

Since current data suggests that ionospheric spatial decorrelation is the most serious threat to WAAS accuracy and integrity, we have constructed a probability model based on the latest experimental data to model our uncertainty regarding the magnitude of "worst-case" ionospheric errors as well as the error magnitudes to be expected under more normal conditions. This model forms the basis for a series of WAAS performance simulations in which accuracy and integrity for users randomly located in the Continental U.S. is measured. Our goal at this stage of WAAS program development is to use computer simulation to project WAAS performance given what is now known. Due to the limited error data and uncertain error models we have now, it is very difficult to meet the performance requirements issued by the RTCA for Category I aircraft precision landing [1,9], but our results under these limitations suggest that it will be feasible to meet the requirements once data from WAAS full-system tests is available in a couple of years.

2.0 Breakdown of WAAS Error Sources

WAAS employs GPS corrections computed by a network of reference stations to remove most of the satellite-based errors that exist without differential corrections. Small errors due to spacecraft clock and ephemeris remain, however, and depending on the *latency* (time to reception) and *age* (time to last usage) of DGPS corrections, Selective Availability (SA) will contribute a ranging error estimated by the simple kinematic relation:

$$SA\ error\ (m) \cong \frac{1}{2} a t^2 ; \qquad a \cong 0.004\ m/\text{sec} \quad (1)$$

where t represents latency plus age, and the "acceleration factor" a has been estimated by studies of SA over time [8]. Using t = 12 seconds as a conservative number for WAAS, this *time-decorrelation* error is very small.

Errors that are *spatially decorrelated* depend on the geographic separation between the user and the site for which the corrections were computed. Local conditions within the ionosphere (about 350 km above the Earth) and the troposphere (the band of the atmosphere from the surface to about 7 miles up) cause variable delays in the GPS ranging signals which distort the true range to the user. These are described in detail in Section 3.0.

Other user-specific errors are due to conditions at or near the user itself, such as multipath (due to reflected ranging signals) and receiver noise. The user should be aware of these local error conditions in order to make good integrity decisions; this is one reason why RAIM is traditionally handled by the user. A summary of the user error model (excluding spatial decorrelation errors) is given in Table 1 [8,13]. The rms of the variances in Table 1 is about one meter. In our WAAS simulations, the effects of these errors are modeled by gaussian noise with a standard deviation of 1 m.

However, for WAAS, the quality of the DGPS corrections is another key integrity factor. The network of remote monitor stations each has backup hardware that computes the corrections independently and looks for any significant discrepancies which might indicate a WAAS hardware or software fault [5]. Flagged faults may lead to non-availability; WAAS applications would not be possible during that time. Unflagged faults could lead to integrity breaches and are thus very serious, as they would affect many users. As a result, WAAS integrity is a dual responsibility of the network and of each individual user.

Error Source	Std. Deviation	Notes
receiver noise	0.5 m	user-dependent
multipath	0.5 m	user-dependent
SV ephemeris	0.4 m	after WAAS
SV clock (w/ SA)	0.3 m	12 sec. lat.+age
ref. survey errors	0.5 m	misc.

Table 1: WAAS Error Source Summary

3.0 Spatial Decorrelation Error Models

The ionosphere layer of the upper atmosphere is awash in charged particles that can affect the timing of messages sent through it. Ionospheric conditions in general are dependent on seasonal and daily variations as well as solar effects, which include an 11-year cycle of waxing and waning solar emissions of charged particles ("solar wind") and the occasional solar flare or other temporary event that creates higher charge levels in the ionosphere. At a smaller scale, charged-particle conditions in the ionosphere will vary from site to site on the globe. GPS ranging signals received by a user are assumed to penetrate the ionosphere at an altitude of 350 km (this penetration point is called a *pierce point*, or PP) and suffer a variable propagation delay in doing so. Note that signals from satellites at lower elevation angles will pass through this layer at a more oblique angle, suffering relatively more time delay. This delay appears as an error to the measured pseudorange for that satellite.

The unaided GPS user relies on the *Klobuchar Model* to adjust for ionospheric conditions based on almanac data contained in the GPS ranging message [4]. This model is accurate to perhaps 15 meters one-sigma, so the remaining error is significant. Differential stations can greatly improve this accuracy because they use high-quality *dual-frequency* GPS receivers to measure the local ionospheric delay to around 0.5 m one sigma (the remainder is primarily T_{gd} *error*). Local-area DGPS systems assume that the user is close enough to the site that is broadcasting DGPS corrections that the variance in the local ionosphere between the user's satellite pierce points and those of the reference station are manageably small. For WAAS, however, the relatively low density of monitor stations across the U.S. means that these distances, or *baselines*, are much larger [6]. Thus, algorithms to model ionospheric delays across a wide area are critical to the overall accuracy of WAAS corrections.

MITRE has proposed the "grid algorithm" to handle ionospheric corrections for WAAS [4]. Basically, the remote monitor stations report their measured ionospheric delays for their satellite pierce points to the master station, which computes vertical (i.e. from a hypothetical satellite directly overhead) ionospheric corrections for each point in a lattice that is superimposed over the U.S. Grid points could be separated by either 5 or 10 degrees of latitude and longitude, although 5 degrees is difficult from a communications standpoint due to the greater number of gridpoint estimates that must be uplinked to the user, who receives the corrections for each grid point as part of the WAAS message. For each of his satellite pierce points, he determines the four grid points that surround it, and then he interpolates the vertical correction at that pierce point using the following equation [4]:

$$Vert.\,Corr. = \sum_{i=1}^{4} I_{est,\,i} \frac{1/d_i}{\sum_{k=1}^{4} 1/d_k} \qquad (2)$$

This vertical correction must be adjusted for the obliquity of that satellite, which can be calculated from its local elevation angle θ and pierce-point elevation θ' using:

$$SF = 1/\sin(\theta') \approx 1 + 2\left[\frac{96 - \theta(\text{deg.})}{90}\right]^3 \qquad (3)$$

Multiplying this factor by the interpolated vertical delay gives the final pseudorange correction for that satellite.

3.1 Ionosphere sampling model

Various researchers have attempted to measure the accuracy of ionospheric corrections of this type using two to four reference stations. In [3], daytime differences between slant ionospheric error predictions at reference stations from 300 to 1800 km apart were measured in 1992-93, when ionospheric conditions were normal apart from a few "stormy" days. In [4,13], grid algorithm corrections were computed based on a network of three reference stations in the Mid-Atlantic area, and the interpolated slant error prediction was compared to the error measured at a fourth station at the assumed user site. This data was taken from Nov. 1992 - July 1993, and again short periods of peak activity were observed.

Using the data in [3,4,13], we have developed a model of ionospheric delay likelihoods that is suitable for WAAS performance simulation. This model gives a distribution for the relative *slant* ionosphere error between two locations as a function of the following factors:

(a) *Solar Cycle*: Most of the experimental data obtained to date is from the early 1990's, which are between the high and low peaks of the current 11-year solar cycle. Delays in peak years would be approximately *double* those measured in these experiments [3]. Similarly, the bottom of the cycle would give delays about half those observed. This is modeled by the following correction factor for solar cycles, CF, which ranges from 0.5 to 2.0:

$$\begin{aligned} CF &= 1+\sin\left(2\pi t_y/11\right) && \text{when } \sin(\bullet)\geq 0 \\ CF &= 1-0.5\sin\left(2\pi t_y/11\right) && \text{when } \sin(\bullet)<0 \end{aligned} \quad (4)$$

In our WAAS simulations, the current date within the solar cycle, t_y, is sampled in the outermost loop by a uniform distribution over an 11-year time span.

(b) *Seasonal*: Slant error results are provided in [3] over three seasonal conditions: winter, summer, and equinox. In addition, the presence of ionospheric storms on a handful of days in 1992-93 is a fourth possible condition. Data for various station separations was collated by seasonal condition to calculate base ionospheric standard deviations for a baseline of 348 km. These two-sigma results and the seasonal probabilities are given in Table 2.

Condition	2σ Deviation	Probability
summer	0.68 m	0.45
winter	1.05 m	0.45
near equinox	1.18 m	0.09
iono. storm	1.85 m	0.01

Table 2: Ionosphere Deviations by Season

Note that local conditions also vary according to the time of day, with the peak deviation occurring at about 2 PM local time, and errors are generally lower at night [3]. This effect is not modeled in our simulations, but given a breakdown of usage times, it could be easily added.

(c) *Baseline*: Data was taken in [3] at various station separations, allowing us to fit a line of ionospheric standard deviation to same-season data over varying-length baselines and then normalizing by a standard 348 km separation. The following linear fit was obtained:

$$RM = 0.416 + \left[0.542\,(\pm 0.06)\right]\frac{range\,(km)}{348} \quad (5)$$

where the (±) factor represents the one-sigma deviation in the slope of the linear fit. Note that the constant factor of 0.416 in this equation, which would exist at a separation of zero, partially represents T_{gd} *error*, which is due to errors in time bias calibration (relative to GPS master time) at the ground monitor sites.

(d) *Tail Distributions*: Data provided in [3] represents 90-99% values of slant ionospheric errors. It is clear from this data that the 99%/90% error ratio is greater than 1.42 as predicted by a Normal distribution. The amount of excess varies between individual data points, but it can be approximated using the standard Normal(0,1) as follows:

$$1.645 \leq \left|z_{samp}\right| \leq 2.33 \quad \Rightarrow \quad TM = 1.13 \pm 0.11 \quad (6a)$$

$$\left|z_{samp}\right| \geq 2.33 \quad \Rightarrow \quad TM = 1.40 \pm 0.25 \quad (6b)$$

$$else \qquad TM = 1.0$$

No breakdowns are given for less than 90% confidence; thus it will be assumed that the distribution of slant delay is Normally distributed between the 5th and 95th percentiles. Between the 1st and 99th percentiles, we continue to use the Normal distribution framework but expand the base variance by multiplying by the (uncertain) TM factor given in equation (6a). In the worst 2% of cases, we multiply by the larger factor given in equation (6b). This is not the most convenient analytical model for ionospheric tail distributions, but it is well suited for Monte Carlo simulations using standard Normal random numbers. Computer simulations of this type allow us the most flexibility in expressing our model's uncertainty.

3.2 WAAS ionospheric sampling procedure

Monte Carlo sampling of this WAAS ionospheric model is conducted in C. The outermost of three loops randomly places an airborne WAAS user within the Continental U.S. by uniformly sampling his latitude and longitude (note that each 2-D point has an approximately equal chance of being chosen). This position is compared to the positions of the 20 proposed ARTCC WAAS remote monitors to measure the relevant separation distances. In the second loop, for each user position,

about one day's worth of GPS satellite geometries is simulated in approximately 15-minute intervals. The Volpe data for the Primary-21 constellation is used, along with four geosynchronous satellites stationed over the equator at longitudes of 180 W, 18.5 W, 55 W, and 63 E. Two of these extra GPS ranging sources are normally visible within the Continental U.S. "Hard failures", which render satellites temporarily unusable, are also simulated for the standard 24 GPS satellites based on the probabilities and procedure given in [7] (also see [10]).

For each GPS geometry, the observation matrix **G** and the vertical dilution-of-precision (VDOP) are computed along with elevation angles for each satellite in view of the user (see [10]). In the innermost loop, 100-200 individual samples of the slant ionospheric error are generated for each satellite in view. Not only does this allow us to tabulate the overall distribution of ionospheric errors, but it allows separate position error computations for each of these inner-loop trials.

For each inner-loop iteration, the current state of the 11-year solar cycle is sampled from a uniform distribution, and CF is computed from equation (4). The seasonal condition is sampled using the distribution in Table 2 to obtain the base sigma, σ_b. Given a baseline distance, we compute the separation modifier RM from equation (5), sampling the uncertain slope parameter when necessary. The ionospheric error variable *z* is sampled from a standard Normal(0,1) distribution, and outcomes outside the 5-95% "normal" range result in the tail modifier TM from equation (6). Finally, since the base data in Table 2 is slant error (not vertical), it already includes an implicit obliquity factor. From the data in [3], a "mean obliquity factor" MO = 1.765 was estimated. This is a necessary approximation which represents the normalized obliquity for the data in [3] based on previous GPS simulations which gave distributions of satellite elevation. The final slant ionospheric error SE is computed as:

$$SE = RM\ CF\ \frac{SF}{1.765}\ TM\ \sigma_b\ z_{samp} \qquad (7)$$

Note that SE represents an error, reported by the nearest "monitor", relative to the "true" ionosphere error of zero that would be obtained with zero spatial decorrelation.

3.3 Troposphere sampling model

Local atmospheric conditions in the troposphere also create transmission delays. Simple models exist for the troposphere, and the WAAS user must rely on them to help correct for this delay [8]. Because the troposphere is closer to the Earth than the ionosphere, the delay error is even more sensitive to satellite elevation than for the ionosphere. Data relating 95% tropospheric errors observed by a WAAS user as a function of satellite elevation is given in Fig. B-1 of [13]. Using two cubic polynomial fits to this data, we can compute the standard deviation for any satellite elevation angle θ (in radians):

$$\sigma_{tr} = -61.23\theta^3 + 55.9\theta^2 - 19.7\theta + 3.045 \quad (\textit{low el.}) \qquad (8a)$$

$$\sigma_{tr} = -0.495\theta^3 + 1.73\theta^2 - 1.99\theta + 0.98 \quad (\textit{high el.}) \qquad (8b)$$

where the boundary for low/high elevation is 18.75 deg. Because tropospheric errors are generally a lesser problem than are ionospheric errors, we do not add tail-probability inflation to this standard deviation. Instead, tropospheric errors are sampled from Normal(0, σ_{tr}) distributions for each satellite pierce point in view. This error is added to the sampled slant ionospheric error from Section 3.3.

3.4 Simulation of DGPS corrections

The spatial decorrelation sampling algorithms can be packaged in various ways to model differing DGPS correction algorithms. The simplest application is local-area, or LADGPS, corrections which are broadcast from the nearest monitor site that can see the satellite in question. The user is thus dependent on a single monitor. Using the ARTCC locations proposed for WAAS, long baselines are possible [6]. For each SV in view of the user, an *independent* slant ionospheric error is generated using (7) based on the distance to the nearest qualified monitor. Tropospheric errors are also sampled, and a sample of the other errors from Table 1 is added. Using the standard GPS observation equations [7], the 3-D and vertical position error can be computed and stored for each trial. Note that for DGPS, the vertical position error is much worse than the two horizontal error components.

Simulating the grid algorithm is much more complex. Without a complete simulation of all WAAS ground operations, an exact model is not possible. Our grid model is designed to represent the essence of interpolation in correcting for spatial decorrelations given the layout of monitor stations on which the gridpoint estimates are based. The grid is composed of 5 or 10-degree cells that cover the geographic area from 10-70 degrees N latitude and 50-160 degrees W longitude. The pierce point of each satellite in view of the user is within one of these grid cells. First, an ideal normalized slant ionosphere error is derived for each grid point by sampling, using (7), given the distance from that grid point to the user. Equation (2) interpolates for the effects of already-sampled grid points (this is a necessary abstraction since no multiple-baseline dependent ionosphere data exists). Another error sampled from (7) is added to each grid point based on the distance from that grid point to the nearest monitor station. Finally, the user's slant ionospheric error is computed by a final interpolation from the four gridpoints using equation (2) and applying the obliquity correction SF/MO. Troposphere and other errors are handled as before, as is the GPS position fix calculation and storage of results.

4.0 Ionospheric Delay: Simulation Results

Although the spatial decorrelation models presented in Section 3.0 are inexact and contain substantial parameter uncertainty, they represent the best knowledge available to

us with the current set of experimental data. The plots that follow show the results of simulations using these models, allowing us to compare and contrast differing DGPS ionospheric correction methods. All the results in this paper contained 2000-5000 user position samples, then 100 GPS geometry samples (over approximately 24 hours) for each user position, then 100-200 spatial decorrelation samples for each spacecraft in view. In other words, 100-200 separate error samples were taken for each user-GPS geometry combination, and each error sample led to a position fix error computation. Overall, 20 to 80 million error samples were conducted, and the entire process took 12-18 hours of CPU time on a Sparc-20.

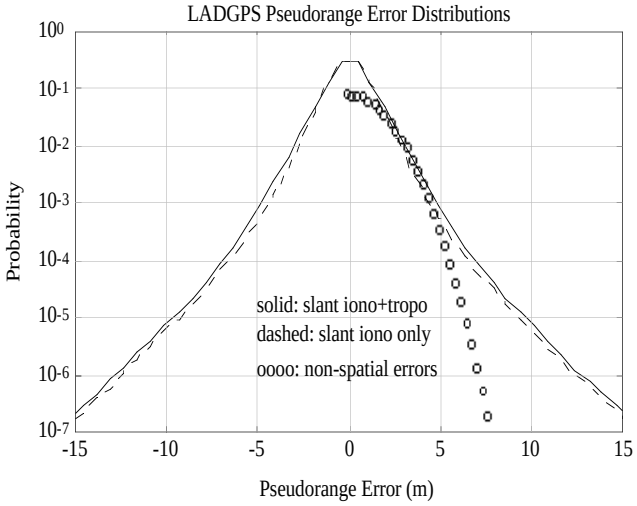

Figure 1: LADGPS Ranging Errors

Figure 1 is a semi-log plot of the density function of slant ionospheric delay for LADGPS, in which only the nearest reference monitor is used for ionospheric corrections. The outer solid line on this "volcano-shaped" plot represents samples of summed ionospheric and tropospheric errors for a given spacecraft. The dashed line inside that represents samples of ionospheric errors only. Note that the ionospheric errors have much larger magnitudes. For comparison purposes, the 'oooo' line represents samples of the non-spatial pseudorange errors from Table 1. Since this is a Normal 1-meter-sigma error, the much more rapid falloff of its tail probabilities illustrates the extent to which the tail distributions of ionospheric errors have been lengthened by our model.

Figure 2 is a similar semi-log plot for the WAAS case in which the MITRE grid algorithm is simulated with 10-degree (solid line) and 5-degree (dashed line) cells. The 10-degree case result is generally 2-10 times better than the LADGPS result in Figure 1, as expected, although the tail-distribution expansion pattern is not much improved. Substantial further improvement in both error magnitude and rare-event spread is gained by using a 5-degree grid. However, a 5-degree grid multiplies the number of needed ionosphere correction points by 4; thus it may overstress the current WAAS communications signal format [8].

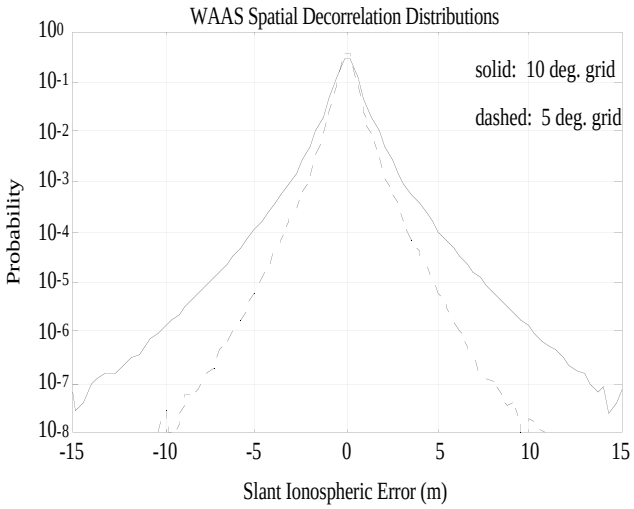

Figure 2: WAAS Slant Ionospheric Error

5.0 DGPS Simulations: Position Error Results

The same simulations that generated the above spatial-decorrelation distributions were used to compute 3-D and vertical DGPS position errors. Vertical position errors dominate this picture and are the most troubling errors for precision aircraft landings. Figure 3 shows the observed cumulative distribution of VDOP from the Inmarsat-augmented and unaugmented GPS geometries sampled. For the basic GPS constellation, VDOP is below 3.2 about 99% of the time. With the extra geosynchronous ranging sources, VDOP ≤ 3.2 occurs 99.87% of the time, and 6 or more satellites are visible 99.9% of the time (using a 7.5-degree user mask angle). These results suggest that very high system *availability* for precision landings, approaching the desired figure of 99.9% set by RTCA, may be possible [1,10]. In our simulations, an availability limit of VDOP = 3.2 was set; i.e. all GPS geometries with higher VDOP were counted as *non-available* for the precision landing application.

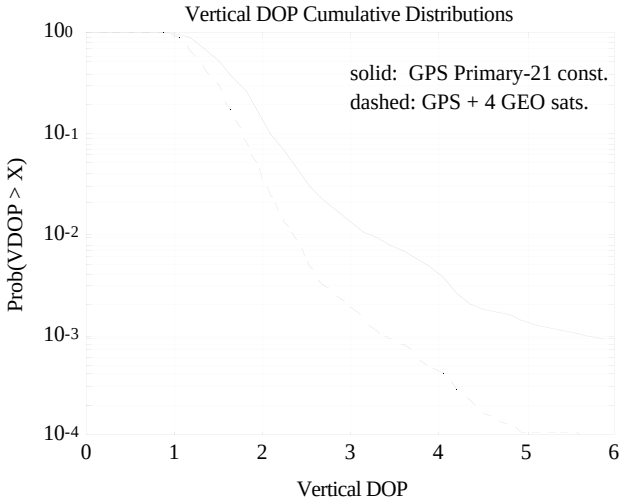

Figure 3: VDOP Simulation Results

Figure 4 plots the density of vertical position errors for the three cases discussed above: LADGPS ('o'), 10-degree WAAS (solid), and 5-degree WAAS (dashed line). The LADGPS plot uses the VDOP = 3.2 limit, which helps limit the position-error effects of rare-event ionospheric errors. However, the two WAAS plots, which are generally superior to those for LADGPS for errors under 25 m, *do not* use this limit for this illustrative simulation run. Without that availability limit, the probabilities of vertical errors stop decreasing past 20 m. From this, it seems that this VDOP limit is the key to limiting the propagations of rare-event spatial decorrelations into unacceptable position errors. Substantial improvements are gained with availability and other RAIM checks, and these will be demonstrated in the following two sections.

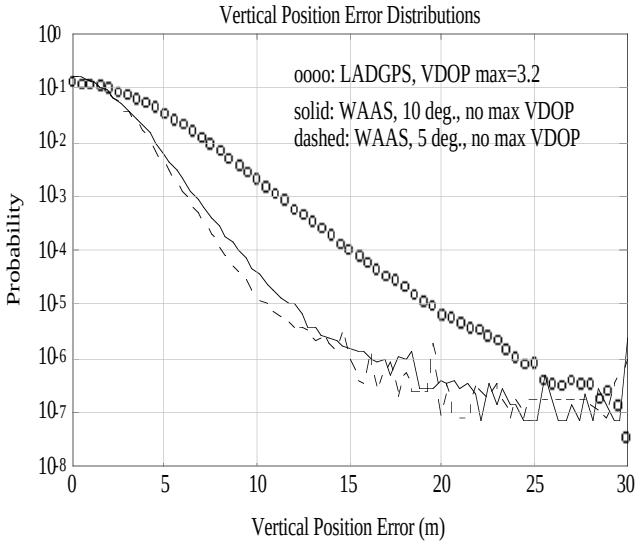

Figure 4: Vertical Position Error Results

The overall results for WAAS are superior to those obtained experimentally by MITRE and Stanford from their 3-station systems [2,13], demonstrating the potential of this 20-station monitor configuration. Furthermore, WAAS is not limited to the configuration under study, as further improvements could be obtained from denser monitor networks and/or more geosynchronous satellites. The effects of these hardware augmentations are now being studied using the simulation procedure developed here.

6.0 WAAS Integrity Methods and Results

6.1 Residuals threshold test algorithm

Given the basic WAAS configuration represented by these simulations, it is possible to apply various integrity algorithms to the simulations in an attempt to further improve the system's accuracy and to warn users of conditions where accuracy risks are unacceptable. This includes availability problems (produced by poor DOP, which is known *a priori*) and continuity and integrity concerns, which result from detected and undetected system faults that occur during a precision approach.

As noted in [7], the standard RAIM algorithm that has been applied to both uncorrected GPS and DGPS consists of a DOP availability check and a *residuals threshold test*. While computing a position fix vector **x** from a vector of pseudorange measurements **z**, a residuals statistic D_n (normalized by the number of spacecraft in view) is computed from the observation matrix **G** as follows [11]:

$$x = G^* z = \left(G^T G\right)^{-1} G^T z \qquad (9)$$

$$D_n \;=\; z^T \left[I_M - G G^* \right] z \;\Big/\; \sqrt{n-4} \qquad (10)$$

The user compares D_n at each position fix step to a preset threshold T, and an *integrity alarm* is issued if $D_n > T$. Various analytical methods for calculating desirable thresholds exist [11], but our research uses the more general user cost optimization developed in [7]. In this approach, a full set of WAAS simulations is conducted, and each resulting set $(\mathbf{x}, D_n)$ is stored as a function of VDOP. Afterward, a simple optimal threshold search is conducted for each VDOP cell to find the threshold that minimizes the *expected user cost*.

A basis for both the RTCA specifications and a cost-based model can be found in the RNP Tunnel Concept for precision aircraft approaches and landings [9]. For a precision approach, integrity decisions must be made close to the ground. The maximum allowable vertical position error for Cat. I precision approach is set at RPE = 15 m. The user costs listed in Table 3 below for *false alarms* (D>T *but* error < RPE), *detected errors* (D > T *and* error > RPE), and *missed detections* (D < T *but* error > RPE) are derived from the allowed risks of an aircraft accident.

RAIM Result	Base Cost	Variable Cost
good position	0	0
detected error	1	0
missed detect.	300	10
false alarm	1.025	0
non-available	0.025	0

Table 3: User RAIM Cost Parameters

Note that the variable cost of a missed detection means that in addition to the base cost of any MD, an additional cost is paid for each "bin" (of width 0.5 m) beyond the RPE limit that the missed position error is located.

In each threshold search, the weighted user cost of the best threshold is compared to the cost of non-availability. If the best threshold cost is lower, then RAIM-supported user position fixes are available for that VDOP. If not, then that VDOP cell is declared to be *non-available*, meaning that the 0.025 cost of non-availability to the user is better than the best result for any threshold for which position fixes could be conducted. Thus, this cost minimization will determine what VDOP should be chosen as the availability limit.

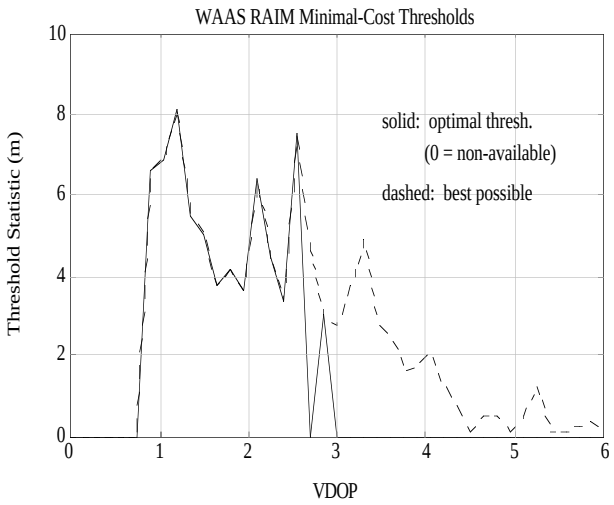

Figure 5: Optimal RAIM User Thresholds

Running this threshold search on the WAAS simulation results in Section 6.0 gives the set of optimal thresholds shown in Figure 5. The discontinuities in the optimal thresholds for adjacent VDOP cells indicate the limited statistical significance of the WAAS Monte Carlo simulation. We expect the best thresholds to uniformly decrease for increasing VDOP, since higher VDOP gives a greater probability of position errors exceeding RPE and thus should lead to more integrity alerts. This result would be realized from an infinite number of simulation trials. Instead of this, simply fitting a line to the optimal thresholds in Figure 5 should be adequate, and the resulting thresholds could then be tested on a longer set of simulation trials. In any case, VDOP greater than 3.0 results in non-availability for this approach, which is close to the limit of 3.2 used in our other algorithms.

Table 4 shows the overall results for this RAIM method. The overall user cost for the optimized RAIM parameters is very low, and we see that the probability of an undetected penetration of the outer precision-landing tunnel is simply Pr(vert. error > 15 m) Pr(MD | vert. error > 15 m) = 2.7 x 10^{-7}. This result is very close to the desired probability of 1 x 10^{-7} as specified in the RNP tunnel concept [9], although it does not necessarily include the effects of all possible ranging errors. For a VDOP limit of 3.0, availability is still very high, and false alarms are infrequent. Overall, these results are very promising and suggest that further improvements to RAIM software can be achieved.

Pr(WAAS available)	0.9958
Pr(false alarm)	0.0005
Pr(vert. error > 15 m)	1.0 x 10^{-6}
Pr(missed detect. | err. > 15 m)	0.2691
Overall User Cost	2.0 x 10^{-6}

Table 4: Residual RAIM Results Summary

6.2 WAAS correction warning algorithms

Another RAIM approach that may be especially suitable for WAAS is based on the very probability models we have built to describe spatial decorrelation errors. Since an airborne WAAS user could possess a similar model, he or she could use it to determine the "believability" of the ionospheric grid corrections received from WAAS. Knowing the positions of visible satellite pierce points within grid cells, the user could potentially flag a satellite whose ionospheric correction looks highly uncertain. Satellites whose corrections have a sufficient uncertainty could be *isolated*, or dropped, from the observation matrix used to compute a position fix. A preliminary version of this idea has been tested and is outlined in this section.

Recall that the user will interpolate an ionospheric correction (call it I_j) for each satellite pierce point from the broadcast grid corrections using equation (2) and then multiplying by the obliquity factor SF from equation (3). From this, an "uncertainty variance" σ_{uv}^2 is computed from the four grid point estimates I_{jk} as follows:

$$\sigma_{uv,j}^2 = \sum_{k=1}^{4} SF_k \frac{\left(I_j^2 - I_{jk}^2\right)}{RM_k^2} \frac{d_1+d_2+d_3+d_4}{d_k} + \sigma_{tr}^2 \quad (11)$$

where SF, RM, and σ_{tr} are defined in equations (3,5,8). Note that the interpolation function (2) has been used to combine the likelihoods of the estimates between the PP and each grid point. A limiting threshold could be set on this statistic, but instead we have tried to project this spatial decorrelation variance from the psuedorange into the vertical position error domain by using this equation:

$$\sigma_{zs,j} = G_{3j}^* \sigma_{uv,j} = \left[\left(G^T G\right)^{-1} G^T\right]_{3j} \sigma_{uv,j} \quad (12)$$

where the (3,j) entry of matrix $\mathbf{G}^*$ is the scalar projection of ranging error into vertical position error. Once we have this statistic for each satellite in view, we perform the following process of checks:

Spatial Decorrelation Isolation Algorithm (SDIA)

(1) *non-available* if VDOP > 3.2
(2) for i = 1,...,n, compute $\sigma_{vs,i}$ and compare to T
(3) if $\sigma_{vs,i}$ > T for any i *and* n > 6, *remove* row i from observation matrix **G** to get $\mathbf{G}_r$
(4) use $\mathbf{G}_r$ to compute position fix *unless*:
    a) VDOP for $\mathbf{G}_r$ > 3.2, *or*
    b) $\sigma_{vs,i}$ > 0.75 T for any other i = 1,...,n
(5) if a) or b) holds, situation is *non-available*

Unlike the residuals RAIM algorithm, it is difficult to choose an optimal threshold T from cost-based search because T is internal to the position-fix computation and must be set before WAAS simulations are run. The

results shown in Figures 6 and 7 below are for T = 4.5 m, which is 30% of the vertical RPE of 15 m.

Figure 6 shows the ionospheric slant delay distributions for a 10-degree WAAS grid. The solid line includes all samples, while the dashed line excludes slant ionospheric errors for satellites that are isolated by the SDIA trial algorithm. Note that the only visible difference is at the rare-event tails of the distribution (beyond errors of ±8 m), where the isolated case probabilities decrease by a factor of 2-10 from the non-isolation distribution. Figure 7 shows the resulting vertical position error distributions.

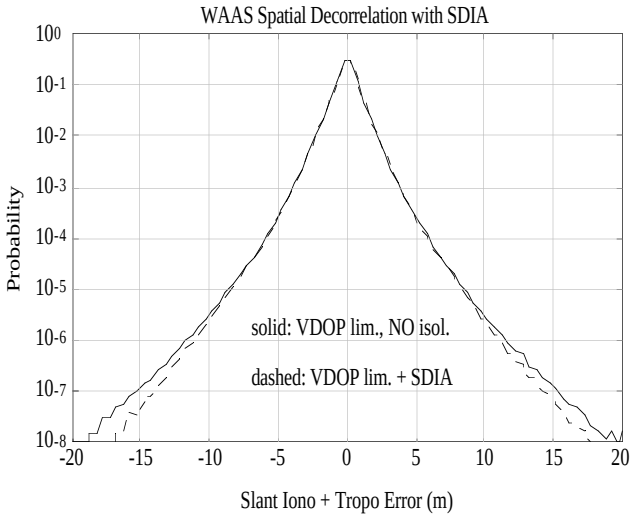

Figure 6: Ranging Errors with Isolations

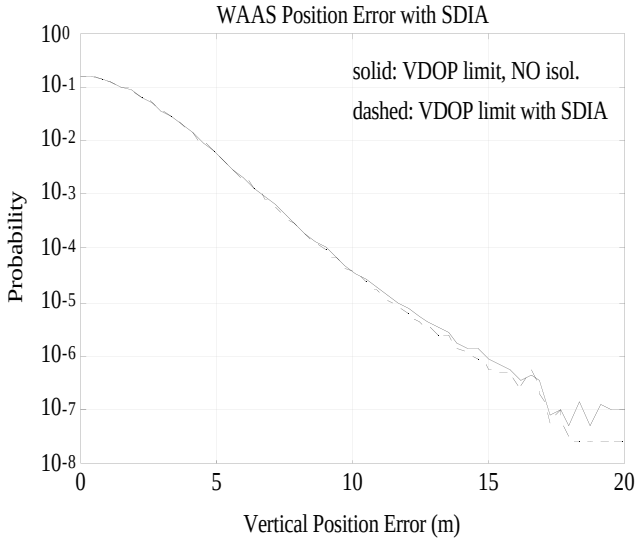

Figure 7: Position Errors with Isolations

Table 5 summarizes the results of WAAS simulations with SDIA. It appears from these results that the improvements gained by using SDIA are noticeable but not decisive. Both excessive position error probability and overall user cost decrease by about 40-50%, and note that SDIA does not hurt availability much at all despite isolating out uncertain-looking satellites 0.5% of the time. This suggests that further reducing the isolation threshold could give better results.

Attribute	With SDIA	Without SDIA
Pr(SV isolation)	0.0051	0
Pr(available)	0.9975	0.9983
Pr(pos err. > 15 m)	1.3×10^{-6}	2.5×10^{-6}
Overall User Cost	0.00046	0.00078

Table 5: SDIA Results Summary

SDIA is but one concept of how this type of isolation could be attempted. It is really only a starting point for the development of more sophisticated algorithms based on the idea of checking observed errors against their prior-probability likelihoods. The WAAS master station will have the role of checking the consistency of the current WAAS corrections and possibly broadcasting an estimate of the variance in the ranging correction for each satellite [5]. This factor could be combined into the user's uncertainty estimates, and it follows that uncertainty models form an important basis for ground-user cooperation in future RAIM procedures for WAAS. Further, it could operate in conjunction with a residuals threshold check on the post-isolation result, since SDIA can be seen as a form of "satellite selection" algorithm to pick and choose from among the visible ranging sources.

While the isolation procedure discussed above is only partially effective to this point, an alternative would be to use the uncertainty model (11,12) in a *weighted-least-squares* position fix computation. This would modify equation (9) in this manner:

$$x_w = \left(G^T W G\right)^{-1} G^T W z \qquad (13)$$

where **W** is an (n x n) matrix of "weights" that express the relative certainty of each measurement source (in this case the satellite pseudoranges) [12]. **W** could be a diagonal matrix of the elements of $1/\sigma_{uv,j}^2$ for j=1,..., n, or it could include ground covariances, etc. Work on this concept (in addition to SDIA) is continuing and being expanded in follow-on research.

7.0 Conclusions and Further Work

This research began with the goal of extrapolating experimental measurements of 95%-bounded ionospheric errors to model uncertain rare-event probabilities for DGPS ionospheric decorrelation errors. The method of estimating the uncertain degree to which tail-probability errors are worse than predicted by a Normal distribution has allowed reasonably efficient Monte Carlo computer sampling of rare-event ionospheric errors, and combining these with samples of other ranging errors has resulted in simulations of vertical position error and other key

performance measures for the proposed WAAS network. These simulations take into account the uncertainty of these extrapolations of experimental data; thus they provide the best possible model of WAAS performance.

Our results show that the proposed 20-station WAAS network and geosynchronous satellite-augmented GPS constellation provide substantially better correction of spatial decorrelation errors for users scattered throughout the Continental U.S. than do local-area corrections. Along with the improved availability of the augmented constellation, user position fix error distributions are much improved, making possible the use of WAAS for Category I aircraft precision landing. The combination of ground integrity information and user RAIM further reduces integrity and continuity errors that could lead to penetrations of the outer tunnel proposed by the RNP [9].

Given the prevailing uncertainty in our error model, a definitive word regarding WAAS integrity, continuity, and availability performance is not yet possible. Spatial decorrelation experiments using more reference stations will provide better and more useful experimental bases for our predictions in the future. Simulations and flight tests which consider communications, software, and other non-physical ranging errors need to be conducted as well. The simulation model developed in this research is now being expanded to consider these other error sources that are unavoidably built into the WAAS architecture.

The most important question remaining in the practical design of an operational WAAS is the marginal utility of (1) improved ground and/or user RAIM software, (2) additional remote monitors, and (3) additional satellites to augment ranging and/or communication. A combination of these should be sufficient to meet all requirements for Category I aircraft precision approach. Our simulations will be used to examine all of these factors. Currently, improved RAIM algorithms (based on those proposed in Section 6.0) are being formulated along with new ideas for ground/user RAIM cooperation. Improved RAIM capability may allow the currently proposed 20-station WAAS network to meet precision landing requirements without further hardware augmentation.

ACKNOWLEDGEMENTS

The authors would like to thank the following people for their help with this research and the software on which it is based: Dr. Clark Cohen, Dave Lawrence, Dr. Changdon Kee, Boris Pervan, and Dr. Todd Walter. The advice and interest of many other people in the Stanford GPS research group are most appreciated, as always.

REFERENCES

[1] P. Enge and A.J. Van Dierendonck, "The Wide Area Augmentation System", *Proc. 8th Int'l. Flight Inspection Symposium*, Denver, CO., June 1994.

[2] T. Walter, C. Kee, Y.C. Chao, Y.J. Tsai, *et.al.*, "Flight Trials of the Wide Area Augmentation System (WAAS)", *Proceedings of ION GPS-94*, Salt Lake City, UT., Sept. 21-23, 1994.

[3] J.A. Klobuchar, P.H. Doherty, and M.B. El-Arini, "Potential Ionospheric Limitations to Wide-Area Differential GPS", *Proceedings of ION GPS-93*, Salt Lake City, UT., Sept. 22-24, 1993, pp. 1245-1254.

[4] M.B. El-Arini and T.C. Wisser, "The FAA Wide Area Differential GPS (WADGPS) Static Ionospheric Experiment", *Proceedings of ION NTM-93*. Anaheim, CA., Jan. 22-24, 1993, pp. 485-496.

[5] R. Loh and J.P. Fernow, "Integrity Concepts for a GPS Wide-Area Augmentation System (WAAS)", *Proceedings of ION NTM-94*, San Diego, CA., Jan. 24-26, 1994, pp. 127-134.

[6] T. Walter, B. Pervan, P. Enge, J. Herendeen, and P. Levin, "Autonomous Integrity Monitoring and Wide Area DGPS", *Proceedings of ION NTM-94*. San Diego, CA., Jan. 24-26, 1994, pp. 485-496.

[7] S. Pullen and B. Parkinson, "A New Approach to GPS Integrity Monitoring using Prior Probabilities and Optimal Threshold Search", *Proceedings of IEEE PLANS '94*. Las Vegas, NV., April 11-15, 1994, pp. 739-746.

[8] P. Enge, "The Global Positioning System: Signals, Measurements, and Performance", *Int'l. J. of Wireless Information Networks*, Vol. 1, No. 2, 1994, pp. 83-105.

[9] J. M. Davis, R. J. Kelly, "RNP Tunnel Concept for Precision Approach with GNSS Application", *Proc. of the ION 49th Annual Meeting*. Cambridge, MA., June 21-23, 1993, pp. 1-20.

[10] W. Phlong, B. Elrod, "Availability Characteristics of GPS and Augmentation Alternatives", *Navigation*, Vol. 40, No. 4, Winter 1993-94, pp. 409-428.

[11] M.A. Sturza, "Navigation System Integrity Monitoring Using Redundant Measurements", *Navigation*, Vol. 35, No. 4, Winter 1988-1989, pp. 483-501.

[12] G.F. Franklin, J.D. Powell, and M.L. Workman, *Digital Control of Dynamic Systems, 2nd Ed.* Reading, MA.: Addison-Wesley, 1990, pp. 374-378.

[13] M.B. El-Arini, C.J. Hegarty, J.P. Fernow, and J.A. Klobuchar, "Development of an Error Budget for a GPS Wide-Area Augmentation System (WAAS)", *Proceedings of ION NTM-94*, San Diego, CA., Jan. 24-26, 1994, pp. 927-936.